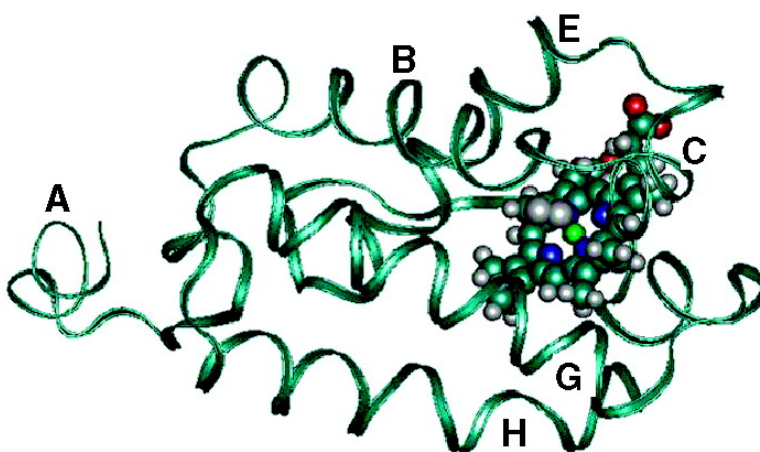Article

Theoretical Study of the Truncated Hemoglobin HbN: Exploring the Molecular Basis of the NO Detoxification Mechanism

Alejandro Crespo, Marcelo A. Mart, Susana G. Kalko, Antonio Morreale,
Modesto Orozco, Jose L. Gelpi, F. Javier Luque, and Daro A. Estrin

More About This Article

Additional resources and features associated with this article are available within the HTML version:

- Supporting Information
- Links to the 11 articles that cite this article, as of the time of this article download
- Access to high resolution figures
- Links to articles and content related to this article
- Copyright permission to reproduce figures and/or text from this article

View the Full Text HTML

Theoretical Study of the Truncated Hemoglobin HbN: Exploring the Molecular Basis of the NO Detoxification Mechanism

Alejandro Crespo,[†] Marcelo A. Martí,[†] Susana G. Kalko,[‡,||] Antonio Morreale,[§] Modesto Orozco,[§] Jose L. Gelpi,[§] F. Javier Luque,*[,‡] and Darío A. Estrin*[,†]

Contribution from the Departamento de Química Inorgánica, Analítica y Química Física/ INQUIMAE-CONICET, Facultad de Ciencias Exactas y Naturales, Universidad de Buenos Aires, Ciudad Universitaria, Pabellón II, Buenos Aires (C1428EHA), Argentina, Departament de Fisicoquímica, Facultat de Farmàcia, Universitat de Barcelona, Av. Diagonal 643, 08028 Barcelona, Spain, and Departament de Bioquímica i Biologia Molecular, Facultat de Química, Universitat de Barcelona, Martí i Franqués 1, 08028 Barcelona, Spain, and Unidad de Modelización Molecular y Bioinformática, Parc Científic de Barcelona, Josep Samitier 1-6, 08028 Barcelona, Spain

Received August 18, 2004; E-mail: dario@qi.fcen.uba.ar (D.A.E.); fjluque@ub.edu (F.J.L.)

Abstract: *Mycobacterium tuberculosis* is the causative agent of human tuberculosis. The nitric oxide reaction with oxy-truncated hemoglobin N (trHbN) has been proposed to be responsible for the resistance mechanism by which this microorganism can evade the toxic effects of NO. In this work, we explore the molecular basis of the NO detoxification mechanism using a combination of classical and hybrid quantum-classical (QM-MM) simulation techniques. We have investigated the structural flexibility of the protein, the ligand affinity properties, and the nitric oxide reaction with coordinated O_2. The analysis of the classical MD trajectory allowed us to identify Phe62 as the gate of the main channel for ligand diffusion to the active site. Moreover, the opening of the channel stems from the interplay between collective backbone motions and local rearrangements in the side chains of the residues that form the bottleneck of the tunnel. Even though the protein environment is not found to make a significant contribution to the heme moiety catalyzed reaction, the binding site influences the physiological function of the enzyme at three different levels. First, by isolating the intermediates formed in the reaction, it prevents nondesired reactions from proceeding. Second, it modulates the ligand (O_2, NO) affinity of the protein, which can be ascribed to both distal and proximal effects. Finally, the stabilization of the Tyr33−Gln58 pair upon O_2 binding might alter the essential dynamics of the protein, leading in turn to a mechanism for ligand-induced regulation.

Introduction

Mycobacterium tuberculosis is the causative agent of human tuberculosis, a disease which infects about one-third of the human population and which causes more than a million deaths per year. Most of those who are infected live in third world countries, where the chances to survive are slim.[1] In healthy individuals, the infection is contained by the immune system, which forces the bacteria into dormancy. It has been reported that nitric oxide and related species are produced in the macrophages during the initial growth infection stage and may be involved in restricting the bacteria in latency.[2] Both endogenous and exogenous NO have been shown to inhibit the development of parasites, such as Trypanosoma, Leishmania,

Plasmodium, and Toxoplasma,[3,4] probably due to the inactivation of parasite cysteine proteases and/or other key enzymes.

The toxic effects of NO can be reduced or even eliminated by the development of resistance mechanisms in microorganisms. One of such mechanisms consists of the oxidation of nitric oxide with heme-bound O_2 to yield the innocuous nitrate ion (eq 1). This mechanism has been found to be operative in bacteria and yeast containing flavohemoglobins.[5,6] The same reaction has been implicated in vertebrate myoglobin and hemoglobin[7,8] and has been proposed to play an important role in the physiology of the recently discovered neuroglobin and cytoglobin heme proteins.[9,10]

† Universidad de Buenos Aires.
‡ Facultat de Farmàcia, Universitat de Barcelona.
§ Facultat de Química, Universitat de Barcelona.
|| Present address: Bioinformatics Unit, IDIBAPS c/Villaroel 170, 08036 Barcelona, Spain.

(1) Bloom, B. R. *Tuberculosis: Pathogenesis, Protection and Control*; ASM Press: Washington D.C., 1994.
(2) MacMicking, J. D.; North, R. J.; LaCourse, R.; Mudgett, J. S.; Shah, S. K.; Nathan, C. F. *Proc. Natl. Acad. Sci. U.S.A.* **1997**, *94*, 5243−5248.

(3) Clark, I. A.; Rocket, K. A. *Adv. Parasitol.* **1996**, *37*, 1−56.
(4) Colasanti, M.; Gradoni, L.; Mattu, M.; Persichini, T.; Salvati, L.; Venturini, G.; Ascenzi, P. *Int. J. Mol. Med.* **2002**, *9*, 131−134.
(5) Gardner, P. R.; Gardner, A. M.; Martin, A. M.; Dou, Y.; Li, T.; Olson, J. S.; Zhu, H.; Riggs, A. F. *J. Biol. Chem.* **2000**, *275*, 12581−12589.
(6) Liu, L.; Zeng, M.; Hausladen, A.; Heitman, J.; Stamler, J. S. *Proc. Natl. Acad. Sci. U.S.A.* **2000**, *97*, 4672−4676.
(7) Eich, R. F.; Li, T.; Lemon, D. D.; Doherty, D. H.; Curry, S. R.; Aitken, J. F.; Mathews, A. J.; Johnson, K. A.; Smith, R. D.; Phillips, G. N.; Olson, J. S. *Biochemistry* **1996**, *35*, 6976−6983.
(8) Ascenzi, P.; Slavati, L.; Brunori, M. *FEBS Lett.* **2001**, *501*, 103−105.

$$Fe(II)O_2 + NO \rightarrow Fe(III) + NO_3^- \qquad (1)$$

M. tuberculosis has been found to encode small heme proteins, referred to as truncated hemoglobins (trHb), which have been proposed to provide protection of bacilli against NO.[11] These proteins are widely distributed in bacteria, unicellular eukaryotes, and higher plants and constitute a distinct group within the hemoglobin superfamily.[12] Thus, they all show very low amino acid sequence homology to vertebrate and nonvertebrate Hbs, with sequence identities <15%.[13] The typical tertiary structure of trHb is based on a two-over-two helical sandwich,[14,15] compared with the three-over-three helical sandwich of the classical Hb fold. The proximal HisF8 heme-linked residue is conserved throughout the Hb and trHb families. The main stabilizing residue in the distal cavity of trHb is typically TyrB10.[14] Two different truncated hemoglobins, known as trHbO and trHbN,[11] are produced by *M. tuberculosis*. While trHbO is expressed during the growth phase, trHbN expression is enhanced during the stationary phase.[11] Recent results from the Bolognesi and Guertin groups show that trHbN appears to be better suited for performing NO/O_2 chemistry, and that it actively detoxifies NO, yielding the innocuous nitrate as product.[14-19]

In this contribution, we have employed state-of-the-art computational classical molecular dynamics (MD) and hybrid quantum-classical (QM-MM) techniques to shed light on the molecular basis for the NO scavenging reaction of oxygenated trHbN from *M. tuberculosis*. To this end, attention has been paid both to the intrinsic fluctuations of the protein and to the details of the heme-controlled oxidation of NO to gain insight into several fundamental issues on the enzyme mechanism. First, how is the channel designed to ensure fast entry of NO into the distal cavity, and how do thermal fluctuations affect its structure? Second, which are the key structural determinants for achieving the large oxygen affinity necessary to guarantee efficient detoxification in hypoxic environments? Finally, which are the main determinants for protein catalysis in the reaction of noncovalently bound NO with the $Fe(II)O_2$ moiety to yield nitrate?

Methods

Classical Molecular Dynamics. Simulations were performed starting from the crystal structure of wild-type oxy-trHbN, at 1.9 Å resolution (PDB entry 1idr).[15] The reported structure is homodimeric, but taking into account the fact that the interface area between the two trHb chains is small,[14] we have performed simulations only for the A subunit. The system was immersed in a pre-equilibrated box of TIP3P water molecules of about $60.0 \times 50.0 \times 70.0$ Å.[20] Water molecules located at less than 2.4 Å from any atom of the protein were removed. Three Na^+ atoms were added to neutralize the system. The final system contains the model protein, 7176 water molecules, and the added ions, leading to a total of 23 518 atoms. Simulations were performed in the NPT ensemble. The system was simulated employing periodic boundary conditions and Ewald sums[21] for treating long-range electrostatic interactions. The optimized system was then heated and equilibrated in three steps: (i) 100 ps of MD heating the whole system from 100 to 200 K, (ii) heating of the entire system from 200 to 298 K for 100 ps, and (iii) equilibration of the entire system for 400 ps at 298 K.

The equilibrated structure was the starting point of a 10 ns MD simulation at constant temperature (298 K). SHAKE was used to keep bonds involving H atoms at their equilibrium length.[22] This allowed us to employ a 2 fs time step for the integration of Newton's equations. Amber99[23] and TIP3P[20] force fields were used to describe the protein and water, respectively. The oxygenated heme model system charges were determined using RESP[24] charges and HF/6-31G(d) wave functions (see Supporting Information). The van der Waals parameters were taken from Amber99. Even if the presence of the transition metal introduces an additional challenge in the simulation, MD simulations are now commonly applied for the investigation of metalloproteins.[25] Frames were collected at 1 ps intervals, giving rise to a total of 10^4 frames, which were subsequently used to analyze the trajectory.

Cavity Calculations. The cavity of the ligand diffusion tunnel was determined using the SURFNET protocol as developed by Laskowski.[26] The shape of the cavity was determined by defining a regular grid of 0.2 Å spacing, where each grid point was assigned a value of 1 (inside the cavity) or 0 (outside the cavity), depending on its accessibility. The 3D matrixes defined by the grids were then used to define the accessible volume.

Classical Molecular Interaction Potential (cMIP). cMIP calculations were used to locate nitric oxide molecules in hidden regions of the protein, as well as to determine the ability of the protein to interact with NO. For this purpose, cMIP[27] calculations were carried out using NO as probe. The origin of the grid was located at the center of the active site (heme group), and a spacing of 0.35 Å was used. The grid was extended long enough to cover the whole channel (approximately 30 Å). A polar grid of 20° was used to study the different orientations of the probe molecule in a given grid element.

Essential Dynamics. The set of structures collected along the 10 ns MD simulation was used to explore the dynamical behavior of the protein. To this end, residues 1−15, which form the N-terminal domain, were excluded since this region was found to be quite flexible (see below), but does not contribute to the structure of the trHb fold or to the definition of the ligand diffusion tunnel. Then, all of the backbone atoms in the rest of the residues were retained and used to superpose the sampled structures. These structures were subsequently used to determine the essential motions, that is, the structural changes that explain more conformational variability in the dynamics of the protein skeleton along the trajectory. To this end, covariance matrixes were built up and diagonalized. The eigenvectors define the type of essential

(9) Pesce, A.; Bolognesi, M.; Bocedi, A.; Ascenzi, P.; Dewilde, S.; Moens, L.; Hankeln, T.; Burmester, T. *EMBO Rep.* **2002**, *3*, 1146−1151.
(10) Pesce, A.; Dewilde, S.; Nardini, M.; Moens, L.; Ascenzi, P.; Hankeln, T.; Burmester, T.; Bolognesi, M. *Structure* **2003**, *11*, 1087−1095.
(11) Couture, M.; Yeh, S.; Wittenberg, B. A.; Wittenberg, J. B.; Ouellet, Y.; Rousseau, D. L.; Guertin, M. *Proc. Natl. Acad. Sci. U.S.A.* **1999**, *96*, 11223−11228.
(12) Moens, L.; Vanfleteren, J.; Van der Peer, Y.; Peeters, K.; Kapp, O.; Czeluzniak, J.; Goodman, M.; Blaxter, M.; Vinogradov, S. *Mol. Biol. Evol.* **1996**, *13*, 324−333.
(13) Couture, M.; Chamberland, H.; St-Pierre, B.; Lafontaine, J.; Guertin, M. *Mol. Gen. Genet.* **1994**, *243*, 185−197.
(14) Pesce, A.; Couture, M.; Dewilde, S.; Guertin, M.; Yamauchi, K.; Ascenzi, P.; Moens, L.; Bolognesi, M. *EMBO J.* **2000**, *19*, 2424−2434.
(15) Milani, M.; Pesce, A.; Ouellet, Y.; Ascenzi, P.; Guertin, M.; Bolognesi, M. *EMBO J.* **2001**, *20*, 3902−3909.
(16) Milani, M.; Pesce, A.; Ouellet, Y.; Dewilde, S.; Friedman, J.; Ascenzi, P.; Guertin, M.; Bolognesi, M. *J. Biol. Chem.* **2004**, *279*, 21520−21525.
(17) Yeh, S. R.; Couture, M.; Ouellet, Y.; Guertin, M.; Rousseau, D. L. *J. Biol. Chem.* **2000**, *275*, 1679−1684.
(18) Ouellet, H.; Ouellet, Y.; Richard, C.; Labarre, M.; Wittenberg, B.; Wittenberg, J.; Guertin, M. *Proc. Natl. Acad. Sci. U.S.A.* **2002**, *99*, 5902−5907.
(19) Mukai, M.; Ouellet, Y.; Ouellet, H.; Guertin, M.; Yeh, S. *Biochemistry* **2004**, *43*, 2764−2770.

(20) Jorgensen, W. L.; Chandrasekar, J.; Madura, J.; Impey, R. W.; Klein, M. L. *J. Chem. Phys.* **1983**, *79*, 926−935.
(21) Luty, B. A.; Tironi, I. G.; van Gunsteren, W. F. *J. Chem. Phys.* **1995**, *103*, 3014−3021.
(22) Ryckaert, J. P.; Ciccotti, G.; Berendsen, H. J. C. *J. Comput. Phys.* **1977**, *23*, 327−341.
(23) Wang, J.; Cieplak, P.; Kollman, P. A. *J. Comput. Chem.* **2000**, *21*, 1049.
(24) Bayly, C. I.; Cieplak, P.; Cornell, W. D.; Kollman, P. A. *J. Phys. Chem.* **1993**, *97*, 10269−10280.
(25) Banci, L. *Curr. Opin. Chem. Biol.* **2003**, *7*, 143−149.
(26) Laskowski, R. A. *J. Mol. Graphics* **1995**, *13*, 323−330.
(27) Gelpí, J. L.; Kalko, S.; de la Cruz, X.; Barril, X.; Cirera, J.; Luque, F. J.; Orozco, M. *Proteins* **2001**, *45*, 428−437.

motions, and the associated eigenvalues determine how much of the positional variance in the trajectory is explained by each eigenvector.[28-31]

QM-MM Calculations. QM-MM calculations[32] were carried out to explore the effect of protein (and solvent) environment in the NO oxidation. There are several QM-MM schemes available, differing mainly in the electronic structure level treatment of the QM subsystem and the force field implemented.[33-37] Here, we employ a novel QM-MM implementation where the QM subsystem is treated at the density functional theory (DFT) level using the efficient SIESTA (Spanish Initiative for the Electronic Structure of Thousands of Atoms) implementation.[38] The SIESTA method has shown an excellent performance for medium and large systems and has also proved to be appropriate for biomolecules and, specifically, for heme models.[39] The use of standard norm-conserving pseudopotentials[38,40] avoids the computation of core electrons, smoothing at the same time the valence charge density. In our study, the nonlinear partial-core correction[41] is applied to the iron atom. Basis functions consisting of localized (numerical) pseudoatomic orbitals are projected on a real space grid to compute the Hartree potential and exchange correlation potentials matrix elements. For all atoms, basis sets of double plus polarization quality were employed, with a pseudoatomic orbital energy shift of 30 meV and a grid cutoff of 150 Ry.[38,39] Calculations were performed using the generalized gradient approximation functional proposed by Perdew, Burke, and Ernzerhof.[42] This combination of functional, basis sets, and grid parameters has been already validated for heme models.[39] The classical subsystem was treated using the Amber99 force field parametrization.[23]

The initial structure for QM-MM calculations was taken from a selected snapshot collected along the classical MD simulation. The NO molecule, which was not considered in the classical MD system, was added at high affinity sites determined from cMIP calculations, close to the heme active site. Since the QM-MM code cannot manage periodic boundary conditions, we solvated this structure with a cap of 7490 water molecules. This structure was thermalized at 300 K. Then, the system was cooled slowly to 0 K and subsequently optimized using Amber99. We have selected the iron porphyrinate plus the NO and O_2 ligands and the axial histidine as the quantum subsystem. The rest of the protein and the water molecules were treated classically. The final system consisted of 50 QM atoms and 24 411 MM atoms. We allowed free motion for QM atoms and for the 809 MM atoms located inside a sphere of 13.5 Å from the QM subsystem center of mass. The frontier between the QM and MM portions of the system was treated by the scaled position link atom method[43,44] adapted to our SIESTA code. Link atoms were used in the proximal histidine to separate the QM-treated imidazole ring from the peptidic backbone. The ferrous unbound pentacoordinated heme group, isolated or in the protein, was treated as a high-spin (HS) quintuplet state, which is known to be the ground state for this system.[45,46] The ferrous O_2 complex was treated as a low-spin singlet state, which is known to be the ground state.[45,46] All species involved in reaction 1 were treated in the low-spin doublet and high-spin quartet states. More technical details about the QM-MM implementation can be found elsewhere.[47]

Ligand affinities (ΔE_L) were calculated using eq 2, where E_{Enz-L} is the energy of the ligand-bound enzyme; E_{Enz} is the energy of the ligand-free enzyme, and E_L is the energy of the isolated ligand.

$$\Delta E_L = E_{Enz-L} - E_L - E_{Enz} \qquad (2)$$

The reaction intermediates formed in the oxidation process of NO to nitrate anion were fully optimized without imposing any constraints. For the model systems used in calculations in vacuum, the minimum energy nature of the stationary points was subsequently verified by normal-mode analysis. Obtaining accurate free energy profiles requires an extensive sampling, which is computationally very expensive and difficult to achieve at the DFT QM-MM level. For these reasons, potential energy profiles were determined using restrained energy minimizations along the reaction path that connects reactant, intermediate, and product states. This procedure, which has provided valuable information in previous QM-MM reaction path calculations,[47] is used here to obtain qualitative insight into the effect of the protein environment and, particularly, on the role played by Tyr33 by comparing the energy profiles obtained for the wild-type enzyme and the Tyr33 → Phe mutant. For this purpose, an additional term was added to the potential energy according to $V(\xi) = k(\xi - \xi_0)^2$, where k is an adjustable force constant; ξ is the value of the reaction coordinate in the system particular configuration, and ξ_0 is the reference value of the reaction coordinate (see below for the choice of the reaction coordinate in the different reactions). When ξ_0 is varied, the system is forced to follow the minimum reaction path along the given coordinate.

Results and Discussion

Structural Flexibility of the Protein. The trHbN protein exhibits the characteristic structural features of the trHb fold, mainly based on the B, E, G, and H α-helices of the classical globin fold (see Figure 1).[14] However, comparison with the sperm whale myoglobin indicates that only 54 C_α pairs can be matched to trHbN, with a root-mean-square deviation of 2.1 Å,[48] which indicates the existence of notable structural deviations. Among the features of the trHb fold that deviate from the classical globin fold, it can be noticed the presence of an extended loop substituting for most of the F-helix, the deletion of the A-helix, which is reduced to a one-turn A-helix tying the N-terminal region to the protein core, and a 12-residue insertion (pre-A region) at the trHbN terminus, which protrudes from the compact protein fold (see Figure 1).[14,15]

MD calculations for the native protein in aqueous solution provide a stable trajectory for the 10 ns simulation time, as can be seen by inspecting the fluctuations in both the potential energy and the positional root-mean-square deviation (RMSD; computed using the subunit A of the crystal structure of 1idr as the reference structure) determined for the heavy atoms in the

(28) García, A. E. *Phys. Rev. Lett.* **1992**, *68*, 2696−2699.
(29) Rueda, M.; Kalko, S. G.; Luque, F. J.; Orozco, M. *J. Am. Chem. Soc.* **2003**, *125*, 8007−8014.
(30) Fradera, X.; Márquez, M.; Smith, B.; Orozco, M.; Luque, F. J. *J. Org. Chem.* **2003**, *68*, 4663−4673.
(31) Wlodek, S. T.; Clark, T. W.; Scott, L. R.; McCammon, J. A. *J. Am. Chem. Soc.* **1997**, *119*, 9513−9522.
(32) Warshel, A.; Levitt, M. *J. Mol. Biol.* **1976**, *103*, 227−249.
(33) Zhang, X.; Harrison, D. H. T.; Cui, Q. *J. Am. Chem. Soc.* **2002**, *124*, 14871−14878.
(34) Ryde, U. *Curr. Opin. Chem. Biol.* **2003**, *7*, 136−142.
(35) Ridder, L.; Harvey, J. N.; Rietjens, I. M. C. M.; Vervoort, J.; Mulholland, A. J. *J. Phys. Chem. B* **2003**, *107*, 2118−2126.
(36) Schöneboom, J. C.; Cohen, S.; Lin, H.; Shaik, S.; Thiel, W. *J. Am. Chem. Soc.* **2004**, *126*, 4017−4034.
(37) Devi-Kesavan, L. S.; Gao, J. *J. Am. Chem. Soc.* **2003**, *125*, 1532−1540.
(38) Soler, J. M.; Artacho, E.; Gale, J.; García, A.; Junquera, J.; Ordejón, P.; Sánchez-Portal, D. *J. Phys.: Condens. Matter* **2002**, *14*, 2745−2779.
(39) Martí, M. A.; Scherlis, D. A.; Doctorovich, F. A.; Ordejón, P.; Estrin, D. A. *J. Biol. Inorg. Chem.* **2003**, *6*, 595−600.
(40) Troullier, N.; Martins, J. L. *Phys. Rev. B* **1991**, *43*, 1993−2006.
(41) Louie, S. G.; Froyen, S.; Cohen, M. L. *Phys. Rev. B* **1982**, *26*, 1738−1742.
(42) Perdew, J. P.; Burke, K.; Ernzerhof, M. *Phys. Rev. Lett.* **1996**, *77*, 3865−3868.
(43) Eichinger, M.; Tavan, P.; Hutter, J.; Parrnello, M. *J. Chem. Phys.* **1999**, *110*, 10452−10467.
(44) Rovira, C.; Schultze, B.; Eichinger, M.; Evanseck, J. D.; Parrinello, M. *Biophys. J.* **2001**, *81*, 435−445.
(45) Scherlis, D. A.; Martí, M. A.; Ordejón, P.; Estrin, D. A. *Int. J. Quantum Chem.* **2002**, *90*, 1505−1514.
(46) Rovira, C.; Kunc, K.; Hutter, J.; Ballone, P.; Parrinello, M. *J. Phys. Chem. A* **1997**, *101*, 8914−8925.
(47) Crespo, A.; Scherlis, D. A.; Martí, M. A.; Ordejón, P.; Roitberg, A. E.; Estrin, D. A. *J. Phys. Chem. B* **2003**, *107*, 13728−13736.
(48) Kachalova, G. S.; Popov, A. N.; Bartunik, H. D. *Science* **1999**, *284*, 473−476.
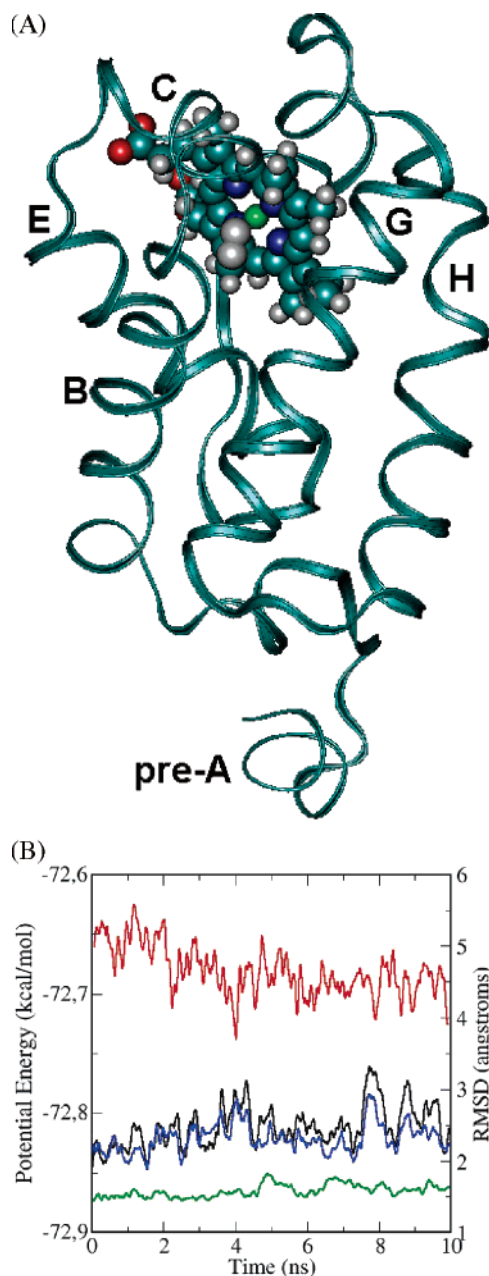
(A)

(B)

Figure 1. (A) Ribbon representation of the structural elements that form the trHb fold. (B) Time evolution of the RMSD (angstroms) of the trHbN protein (blue), the N-terminal region (residues 1−15; black), and the protein core (green), which includes the heme active site, as well as the total potential energy of the entire system (kcal/mol; red).

protein along the simulation (Figure 1). It is worth noting that a large fraction of the structural flexibility stems from the N-terminal (residues 1−15) region, whose RMSD (around 2.6 Å) accounts for most of the total protein RMSD (see Figure 1). This enhanced flexibility can be realized from the lack of the elongated α-helix expected in a conventional Hb fold, the protrusion of the N-terminal region from the protein core, and the favorable hydration of the highly polar sequence motif in the 6−11 (Arg-Leu-Arg-Lys-Arg-Glu) pre-A region. In contrast, the main fold of the protein core (residues 16−127), which comprises the heme active site, is well preserved and exhibits smaller RMSD values (around 1.6 Å).

To gain insight into the dynamical behavior of trHbN, the essential motions of the protein core were examined by diag-
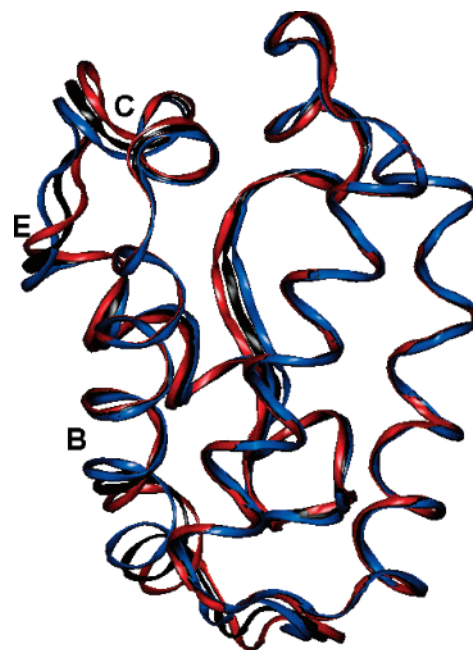

Figure 2. Ribbon representation of the structural displacement of B- and E-helices in trHbN originated from the first essential motion of the protein core backbone. The figure represents the average backbone structure of the protein core (black), as well as those structures (red and blue) corresponding to the maximum displacements along the first essential movement.

onalizing the positional covariance matrix determined for the backbone atoms (see Methods). The calculated eigenvalues decrease in magnitude smoothly, thus indicating that a variety of motions determine the structural flexibility of the protein backbone, as noted previously for other proteins.[48−52] Thus, nearly 44% of the backbone conformational flexibility is accounted for when the 10 principal components are considered, and only the first three normal motions contribute separately more than 5% to the structural variance of the backbone. The first essential movement (8% of structural variance) mainly involves the relative motion of the B- and E-helices (see Figure 2). The second principal motion (7.3%) mostly affects helix C and the hinge regions between E−F- and F−G-helices. Finally, the third component (6.4%) involves fluctuations in the hinge region between B- and C-helices, as well as displacements in B-, G-, and H-helices. Overall, these results indicate that the backbone fluctuations in trHbN arise from a complex interplay of movements which involve the different secondary structure elements.

As noted by Bolognesi and co-workers,[14,15] one of the most striking features in trHbN is the presence of an almost continuous tunnel through the protein matrix that connects the heme distal pocket to the protein surface at two distinct sites. The tunnel is composed by two orthogonal branches, stretching around 20 and 8 Å, respectively, from the access sites to the heme ligand site. The inner surface of the largest tunnel branch is mainly defined by apolar residues pertaining to the B- (Ile19, Ala24, Ile25, Val28, Val29, Phe32) and E- (Phe62, Ala63,

(49) Englander, S. W.; Kallenbach, N. R. *Q. Rev. Biophys.* **1983**, *16*, 521−655.
(50) Wuthrich, K. *Q. Rev. Biophys.* **1987**, *19*, 3−5.
(51) Amadei, A.; Linssen, A. B.; Berendsen, H. J. *Proteins* **1993**, *17*, 412−425.
(52) McCammon, J. A.; Harvey, S. C. *Dynamics of Proteins and Nucleic Acids*; Cambridge University Press: New York, 1987.
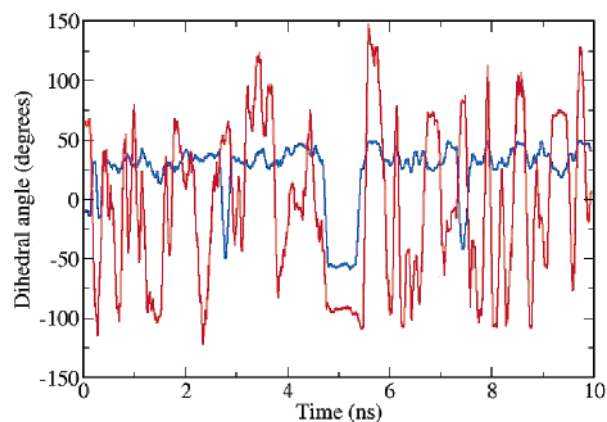
Figure 3. Time evolution of the Phe62 $C_\alpha-C_\beta$ (blue line) and $C_\beta-C_\gamma$ (red line) dihedral angles.

Leu66) helices. For the shortest branch, it also involves apolar residues in G- (Ala95, Leu98) and H- (Leu116, Ile119) helices.

Inspection of the fluctuations experienced by those residues along the simulation revealed that the opening of the passage through the tunnel is mainly controlled by Phe62, a residue which lies close to Phe32 and Leu98. In fact, the analysis of the MD simulation showed that Phe62 populates two main conformations, which are characterized by average torsional angles around the $C_\alpha-C_\beta$ bond of about 35 and $-50°$ (Figure 3). Interestingly, Milani et al.[15] have pointed out that this residue is also observed in two alternate conformations differing by $\sim63°$ by rotation around the $C_\alpha-C_\beta$ bond in the X-ray crystallographic structure. When the $C_\alpha-C_\beta$ torsional angle is close to 35°, which is the most populated conformation sampled along the trajectory, there is no apparent restriction to the conformational flexibility around the $C_\beta-C_\gamma$ bond (see Figure 3). However, when the $C_\alpha-C_\beta$ dihedral angle is close to $-50°$, the conformational flexibility around the $C_\beta-C_\gamma$ bond is more restricted, which can be attributed to unfavorable contacts with Ile25 and Ile119.

The analysis of the MD trajectory also revealed that the adoption of two different conformations around the $C_\alpha-C_\beta$ torsional angle of Phe62 is crucial for the opening of the channel leading to the active site. Thus, when the torsion around the $C_\alpha-C_\beta$ bond is $\sim35°$, the phenyl ring of Phe62 enters the ligand diffusion tunnel and impedes the access of the ligand to the active site. However, when the dihedral angle around the $C_\alpha-C_\beta$ bond changes from ~35 to approximately $-50°$, the benzene ring roughly lies parallel to the axis of the tunnel and there is a drastic reduction in the steric hindrance for the ligand diffusion through the tunnel. This is reflected in the distance from Phe62 to Phe32, which is generally in the range of 3−5 Å in the former conformation, but it increases up to 9 Å when such a conformational change takes place (see Figure 4). These two conformational states might, therefore, be associated to *closed* and *open* states of the channel. In the closed conformation, the tunnel volume amounts, on average, to ~350 Å^3, which is similar to the value obtained for the X-ray crystallographic structure.[15] The transition from the closed state to the open one is associated with an increase in the tunnel volume, which amounts, on average, to ~78 Å^3, a value somewhat smaller than the range of van der Waals volumes typically assigned to methylbenzene (from 95 to 102 Å^3).[53] On the other hand, such a conformational
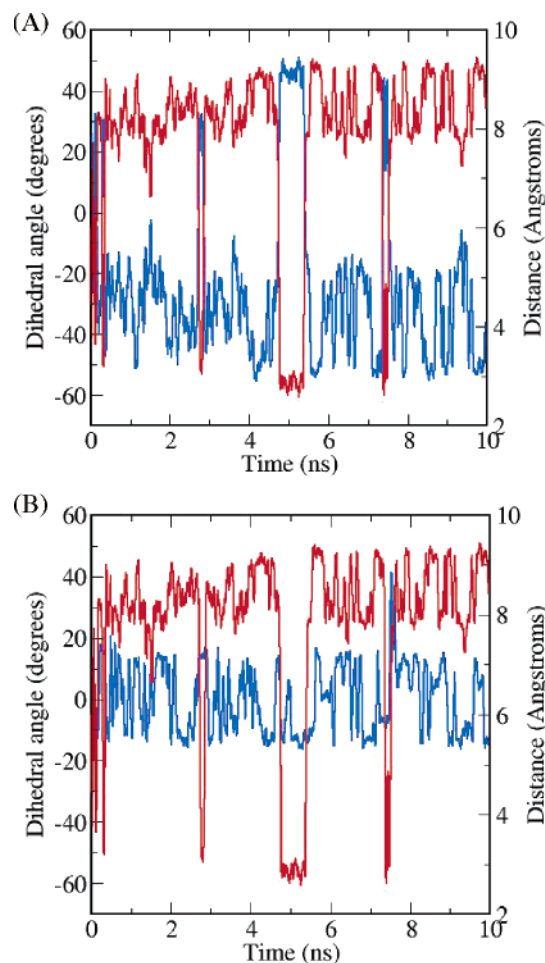

Figure 4. Time evolution of the Phe62 $C_\alpha-C_\beta$ dihedral angle (red line), and of the distances from (A) Phe62 and Phe32 (blue line; measured from atom HZ in Phe62 to atom HE21 in Phe32) and (B) Phe62 and Leu98 (blue line; measured from atom HZ in Phe62 to atom HD21 in Leu98).

transition increases the width of the tunnel, which is found to reach values up to ~3.4 Å, as determined from the shortest contact distance between the van der Waals surfaces of the residues that define the bottleneck of the tunnel.

The finding that the adoption of the two conformations around the $C_\alpha-C_\beta$ bond leads to open and closed configurations was further verified by delineating the channel by using 3D grids defined according to Laskowski's method (Figure 5).[26] For the open conformation, the surface of the channel leading from the heme group to the outer space is well defined, without discontinuities. Moreover, it clearly shows that the adoption of the open conformation leads to opening of the two branches of the tunnel leading to the heme binding site. In contrast, the walls of the cavity are broken in those snapshots where Phe62 adopts a closed conformation (Figure 5).

Similar findings can be obtained from inspection of the isocontour plots determined from cMIP calculations for the interaction of a NO probe with the protein. Calculations performed for both open and closed states of the protein reveal the existence of a favorable interaction energy region in the distal side of the heme group, located between the iron atom and Tyr33 (Figure 6). Such a region also protrudes toward the

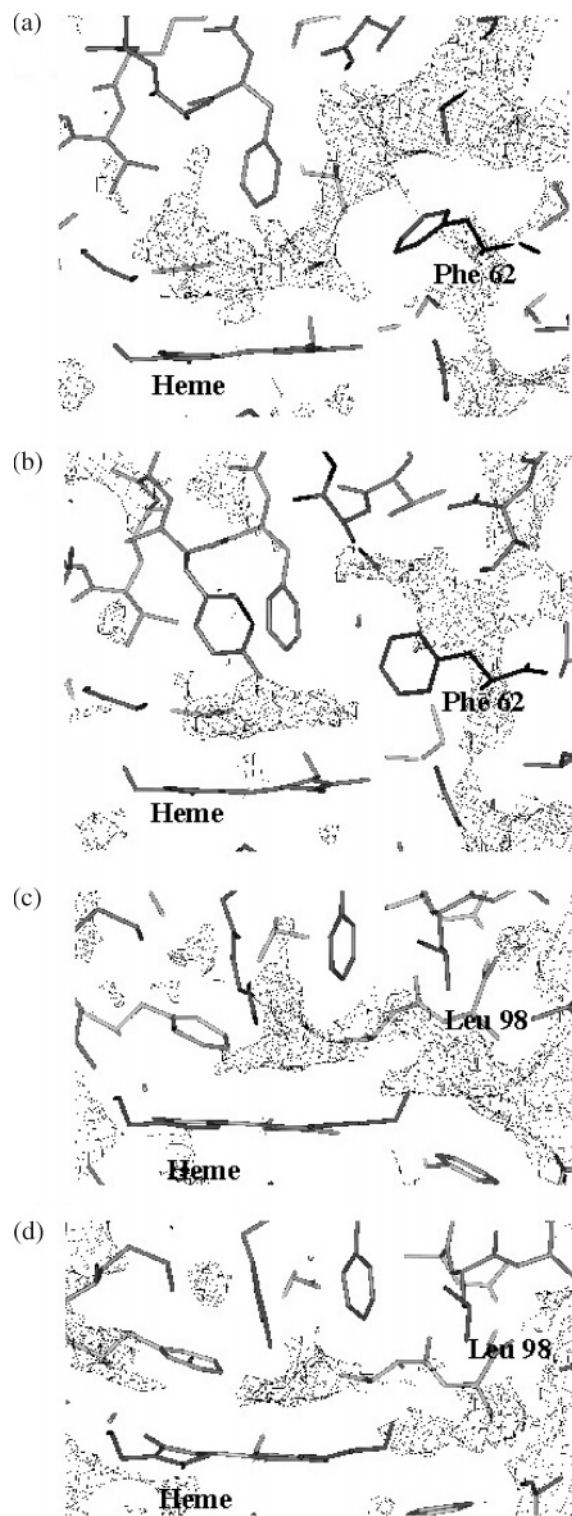(53) Gogonea, V.; Osawa, E. *J. Comput. Chem.* **1995**, *16*, 817−842.

(a)

(b)

(c)

(d)

Figure 5. Representation of the ligand diffusion tunnel in trHbN. A and B correspond to views of the largest branch of the tunnel in the open and closed channel conformations, respectively, whereas C and D show the corresponding views for the shortest branch of the tunnel in the open and closed conformations.
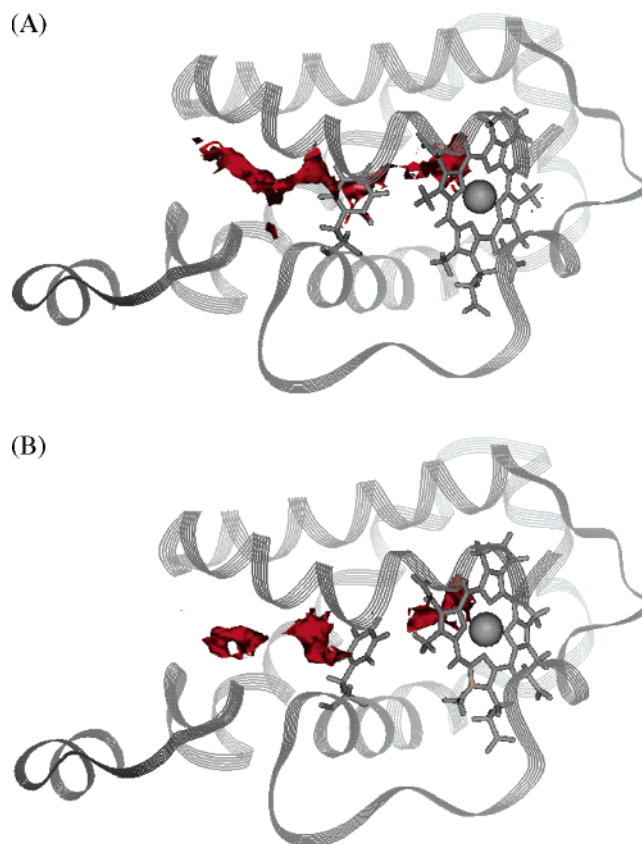
(A)

(B)

Figure 6. Isocontour plots corresponding to the interaction energy between the NO probe and the protein determined from classical molecular interaction potential (cMIP) calculations for selected snapshots representative of the open (A) and closed (B) conformations, which are shown in comparable orientations. Calculations were carried out in the absence of the O_2 molecule. Both Phe62 and the heme group (with the iron atom represented by a sphere) are explicitly displayed. Contour plots correspond to -2 kcal/mol.

intersection of the two tunnel branches, thus occupying a space in the cavity that coincides with one of the secondary Xe binding sites recently found by Bolognesi's group upon treatment of trHbN crystals under Xe pressure.[16] There is, however, a fundamental difference in the isocontour plots determined for the open and closed conformations of the protein. When the

protein adopts an open conformation (see Figure 6, top), there is a continuous energy isocontour that delineates the channel leading from the tunnel entrance to the heme binding site. In contrast, for those structures corresponding to the closed state, such an energy isocontour is broken due to the phenyl ring of Phe62, which enters the long branch of the tunnel (see Figure 6, bottom). In this latter case, it is worth noting the existence of a favorable interaction energy region located in the tunnel long branch facing the Phe62 benzene ring, which is also in agreement with the main Xe binding site recently identified by Bolognesi et al.[16]

The preceding findings point out that the main bottleneck for the passage of ligands through the channel comes from the relative arrangement between the side chains of Phe32, Phe62, and Leu98, which pertain to E-, B-, and G-helices, respectively. Moreover, Phe62 can be considered to be the gate of the main channel leading to the heme group in the active site. Even though the limited length of the simulation precludes performing a statistical analysis of the ratio between the population of open and closed conformations of the channel, inspection of Figure 4 clearly points out that the conformational change around the $C_\alpha-C_\beta$ bond of Phe62 is not a rare event. In fact, several conformational transitions occurred spontaneously along the simulation, and in one case, the main channel remained in the open configuration for around 0.8 ns. Those transitions can be expected to originate from the fluctuations in the protein structure, which can be characterized in terms of the separate

essential motions (see above) that determine the intrinsic flexibility of the protein. It is, therefore, reasonable to expect that when those essential motions act in a concerted way and have the appropriate magnitude, the collective structural fluctuation experienced by the protein backbone might trigger the conformational change in Phe62, thus leading to the transition between open and closed states.

To explore the connection between the local motions of the side chain of Phe62 and the essential motions that modulate the structural fluctuations of the protein backbone, we determined the correlation between the displacements of the backbone C_α atoms and the fluctuation in the distance from Phe62 to either Phe32 or Leu98. This was accomplished by using eq 3,[54] where $r_{\tau i}$ is the correlation coefficient between the $\tau(t)$ ($\tau = x$, y, or z) coordinates of the C_α atom of residue i at time t, and $\rho(t)$ denotes the distance between residues.

$$r_{\tau i} = \frac{\langle(\tau_i(t) - \langle\tau_i\rangle_t)(\rho_i(t) - \langle\rho_i\rangle_t)\rangle}{\sqrt{\langle(\tau_i(t) - \langle\tau_i\rangle_t)^2\rangle_t\langle(\rho_i(t) - \langle\rho_i\rangle_t)^2\rangle_t}} \qquad (3)$$

No significant correlation was found when the inter-residue distance parameters, $\rho(t)$, were compared with the position of the C_α atoms projected along each of the main principal components that define the essential dynamics of the protein. This indicates that the fluctuations between the residues that define the bottleneck in the ligand diffusion tunnel cannot be attributed to a specific motion between structural elements. A clear correlation was, however, found between the fluctuations in the Phe62−Leu98 distance and the positional displacements of the C_α atoms for ∼50% of the residues in the protein, mainly pertaining to helices B, C, and F and segments of helices E and H. This finding, therefore, suggests that the opening of the channel between residues Phe62 and Leu98 stems from a concerted motion of a large fraction of the protein. Finally, no clear correlation was found between the Phe62−Phe32 distance and the positional fluctuations of the C_α atoms. This finding suggests that the mechanism leading to opening of the passage through the ligand diffusion tunnel stems from the interplay between collective motions of the protein backbone and changes in dihedral angles of specific residues, particularly Phe62, which would eventually facilitate the transition from the closed conformation to the open one.

Finally, we have analyzed the structural fluctuations in the vicinity of the heme active site. The O_2 molecule bound to the Fe atom interacts with Tyr33 through a hydrogen bond along the whole trajectory (average OH−O1 and OH−O2 distances of 3.27 and 2.76 Å, respectively). This interaction has been proposed to play an important role in the stabilization of the heme-bound oxygen.[17] On the other hand, a much weaker interaction is found between O_2 and Gln58 (average NE−O1 and NE−O2 distances of 3.67 and 3.82 Å, respectively), which is in agreement with the experimental evidence.[15] In fact, the analysis of the MD trajectory revealed a hydrogen-bond contact between Gln58 and Tyr33 (average NE−O distance of 3.00 Å). These results, therefore, give support to the suggestion[14,15] that Gln58 is crucial in the detoxification reaction because it might interact with the NO molecule and contribute to correctly
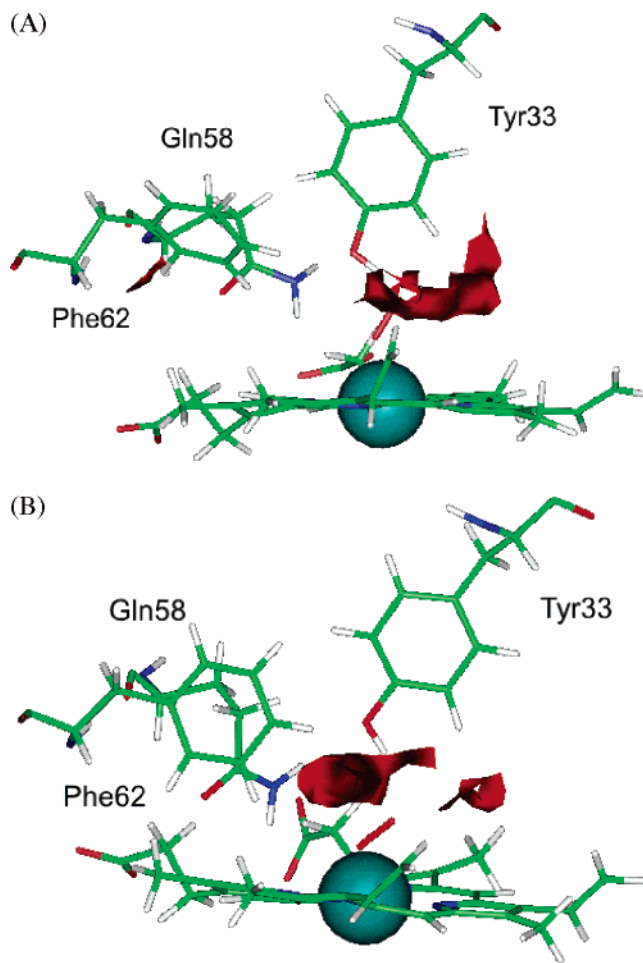
(54) Shen, T.; Tai, K.; Henchman, R. H.; McCammon, J. A. *Acc. Chem. Res.* **2002**, *35*, 332−340.

(A)

(B)

Figure 7. Isocontour plots corresponding to the interaction energy between the NO probe and the O_2-bound form of the trHbN enzyme determined from classical molecular interaction potential (cMIP) calculations for selected snapshots representative of the open (A) and closed (B) conformations. Besides Tyr33, Gln58, and Phe62, the plots display the oxygen molecule (in red) and the heme group with the iron atom represented by a sphere. Contour plots correspond to −3 (open) and −2 (closed) kcal/mol.

positioning NO to react with O_2. At this point, cMIP calculations performed for selected snapshots in both open and closed conformations reveal the existence of a region favorable for the interaction with the NO probe in the proximity of the bound O_2 (see Figure 7). In fact, such a region corresponds to the most favorable interaction site for the NO probe in the whole ligand diffusion tunnel.

Effect of the Environment on the O_2 Affinity of the Heme Group. A requirement to grant survival of *M. tuberculosis* under hypoxic conditions when the bacilli enter latency is the high O_2 affinity of the enzyme ($P_{50} \approx 0.01$ mmHg), which has been attributed to the interaction of the bound oxygen with Tyr33.[11] Following previous studies,[55] our main interest here is to explore by means of electronic structure calculations the influence of the protein environment in modulating the O_2 binding to the trHbN enzyme. To this end, the geometrical and energetic features of the interaction between oxygen and the heme group in vacuum, the wild-type (wt) protein, and the Tyr33 → Phe mutant have been determined. Table 1 reports selected properties for the bound and unbound states of the heme group in the preceding systems.

(55) Scherlis, D. A.; Estrin, D. A. *J. Am. Chem. Soc.* **2001**, *123*, 8436−8437.

Table 1. Relevant Geometrical Parameters (distances in angstroms and angles in degrees), Changes in Mulliken Charges (in units of electron), and Energetical Changes (ΔE; in kcal/mol) for the Binding of O_2 to the Heme Group (Hem + O_2 → Hem–O_2) in Vacuum, in the Wild Protein, and in the Tyr33 → Phe33-Mutated Protein Determined from QM-MM Calculations[a]

	Vacuum		Wild Type TrHb		Tyr33 → Phe33 (mut)	
	oxy	free	oxy	free	oxy	free
Fe–O1	1.78		1.84 (2.19, 2.06)		1.86	
O1–O2	1.29		1.31 (1.20, 1.20)		1.31	
Fe–O1–O2	121.7		120.7 (122.4, 114.2)		120.4	
O2–Tyr33$_{OH}$			2.75 (3.17, 3.09)			
O1–Gln58$_{NE}$			3.52 (3.86, 3.77)		3.37	
Tyr33$_{OH}$–Gln58$_{NE}$			2.98 (3.13, 2.83)	2.99		
Fe–His81$_{NE}$	2.12	2.16	2.06 (2.10, 2.11)	2.13	2.09	2.10
Fe–Hem:N$_{plane}$	0.04	−0.27	0.02 (0.02, 0.02)	−0.25	0.02	−0.29
His81: tilt angle	88.1–90.4	97.9–98.5	87.6–91.9 (88.1–91.5, 89.2–92.0)	94.9–101.4	87.8–92.2	94.3–102.7
His81: rotation angle	12.4	13.7	33.9 (29.0, 29.0)	33.6	28.7	27.7
Δq(O$_2$)	−0.20		−0.36		−0.35	
Δq(His81)	0.16		0.21		0.22	
ΔE	−21.4		−37.2		−34.3	

[a] Experimental values for the wt oxygenated protein (A and B chains) reported in ref 15 are given in parentheses.

For the isolated heme group, the binding energy amounts to −21.4 kcal/mol, which is somewhat lower than the binding energy reported by Rovira et al. from BLYP computations.[46] In trHbN, calculations predict a substantial increase (by around 16 kcal/mol) of the O_2 binding, though the distance from the Fe atom to the O_2 is increased by 0.06 Å (a distance of 1.84 Å is found for the wt enzyme; see Table 1)[56] compared to that in the model system in vacuum. Despite the uncertainties that might arise from the computational approach used to estimate the binding energies, the preceding result supports the crucial role played by the protein environment in modulating the O_2 affinity. Particularly, the hydroxyl group of Tyr33 is hydrogen bonded to O_2, with a distance between the hydroxyl oxygen and the O_2 molecule of 2.75 Å, thus supporting the implication of Tyr33 in assisting the binding of O_2. To further examine the specific role played by Tyr33, we have determined the binding of O_2 for the Tyr33 → Phe mutant. Though the Fe···O_2 distance remains little affected, the binding energy in the mutant is around 3 kcal/mol smaller than that for the wt protein, which agrees qualitatively with the ~150-fold increase in the O_2 dissociation rate in the mutant.[11,17]

Several studies in model heme compounds[57,58] have pointed out that the O_2 binding might be modulated through another mechanism which exploits the hydrogen bond formed between the proximal His81 and the carbonyl group of Met77 (1.77 Å in the optimized structure for the wt enzyme; see Figure 8). Such a hydrogen bond augments the donation capacity of His81,
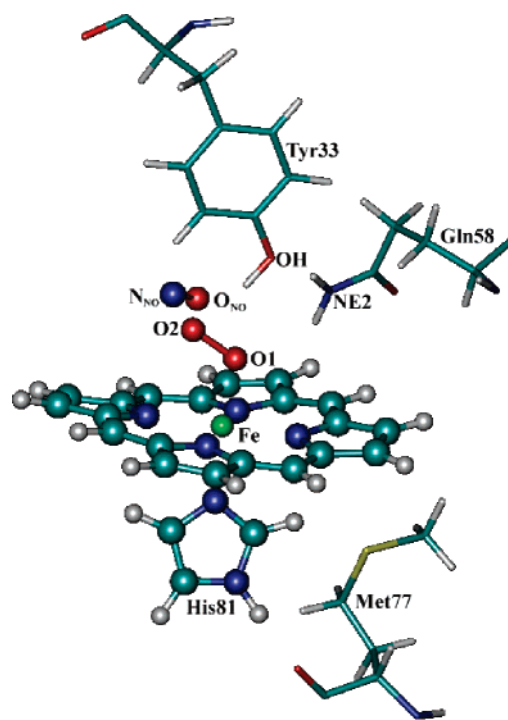
(56) The experimental X-ray structure was solved at 1.9 Å resolution, which implies a mean error in atomic coordinates of about 0.1 Å. However, differences between 0.1 and 0.3 Å for the selected geometrical parameters shown in Table 1 are found in the two subunits of the X-ray crystallographic structure. Particularly, the larger value found for the Fe–O1 distance in 1IDR (2.06 and 2.19 Å) relative to other oxygenated heme proteins (myoglobin 1MBO = 1.83 Å; ascaris hemoglobin = 1.90 Å) might reflect, at least in part, differences in the restraints used in the crystallographic refinement (M. Bolognesi, personal communication).
(57) Kundu, S.; Snyder, B.; Das, K.; Chowdhury, P.; Park, J.; Petrich, J. W.; Hargrove, M. S. *Struct. Funct. Genet.* **2002**, *46*, 268−277.
(58) Jain, R.; Chan, M. K. *J. Biol. Inorg. Chem.* **2003**, *8*, 1−11.

Figure 8. Relevant numbering representation of the trHbN active site (QM atoms are depicted using ball-and-stick motif).

increasing the Fe–His bond strength and, in turn, reinforcing the Fe–O_2 bond. This mechanism is supported by the results given in Table 1 since the optimized His–Fe coordination bond decreases by 0.06 Å in trHbN compared to that in the model system in vacuum. Indeed, the net Mulliken charge on the oxygen is also consistent with the strength of the bond (−0.20 and −0.36 e in vacuum and in the protein, respectively), showing a larger degree of back-donation from the metal in the latter case. Finally, the net positive charge on the proximal histidine is significantly larger in the protein compared with

that in the isolated model system, confirming the enhanced donor capacity of this residue arising from hydrogen bonding to Met77. To quantify this effect, we performed an additional QM-MM calculation in which proximal electrostatic interactions were annihilated, thus eliminating the C=O Met77−His81 hydrogen-bond interaction. The computed oxygen affinity was reduced by 1.8 kcal/mol, showing that the hydrogen-bond effect is small but significant.

NO Reaction with Coordinated O₂. The interaction of NO with the O_2-bound heme group was examined by using selected structures obtained from cMIP calculations (see above and Figure 7) as starting configurations for the QM-MM calculations. After QM-MM optimization, the NO molecule was best placed in the active site close to O_2 and interacting with Tyr33 and Gln58 residues (N_{NO}−O2 = 2.99 Å, N_{NO}−Tyr33HH = 3.17 Å, and O_{NO}−Gln58HE21 = 2.90 Å). The oxidation reaction of NO was investigated considering a mechanism in which a peroxynitrite ion is formed from the attack of NO to the coordinated O_2. Subsequently, the metal center catalyzes the isomerization of peroxynitrite to nitrate. This latter process has been reported to proceed rapidly in both model systems[59,60] as well as in myoglobin and hemoglobin.[61] Calculations were performed for the isolated model system (vacuum), for the same model system solvated in aqueous solution (by using a cluster of 1061 water molecules), in the wt protein, and in the Tyr33 → Phe33 mutant.

According to the preceding mechanism, we first investigated the NO addition to the coordinated O_2 to yield peroxynitrite (eq 4). The proposed concerted mechanism was analyzed using restrained energy minimizations along the selected reaction coordinate, the distance between the nitrogen of NO and one oxygen atom ion, $\xi_1 = d(O_2 - N_{NO})$ (Figure 8).

$$Fe(II) - O_2 + NO \rightarrow Fe(III) \; [-OONO] \qquad (4)$$

The reaction proceeds barrierless in all cases considered in the QM-MM calculations (see Figure 9A). The computed ΔE values were found to be −14.6, −20.0, −23.0, and −21.5 kcal/mol for vacuum, water, wt protein, and mutant, respectively. The reaction involves the formation of a bond between O1 and the N atom of NO and the weakening of both O1−O2 and N−O bonds, as can be seen from the structural parameters shown in Table 2. There are no significant differences between the geometrical features of reactants and products in going from vacuum to protein. It is interesting to note that the O1−O2 bond distance in the resulting coordinated nitrite is longer than the one corresponding to the isolated species (1.38 Å). This is consistent with the fact that coordination to heme weakens this bond and, therefore, favors isomerization to nitrate anion. However, it is clear that the protein environment around the heme group does not play a significant role in catalyzing the formation of nitrate.

The spin populations and Mulliken charges for selected groups for the reaction in the protein environment are given in Table 3. As expected, in the reactants, the unpaired electron is mainly located on the NO moiety. The electronic structure of the Fe−O₂ complex shows the antiferromagnetic coupling of two regions of opposite spins, which is in agreement with
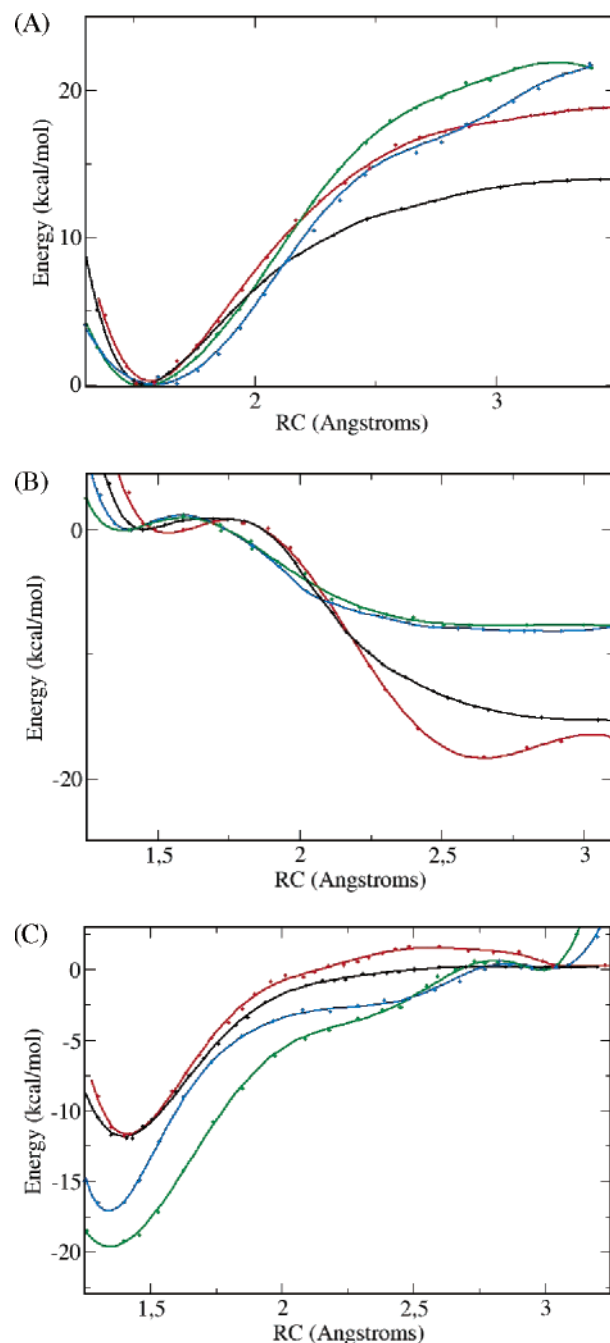
(59) Jensen, M. P.; Riley, D. P. *Inorg. Chem.* **2002**, *41*, 4788−4797.
(60) Shimanovich, R.; Groves, J. T. *Arch. Biochem. Biophys.* **2001**, *387*, 307−317.
(61) Herold, S.; Shivashankar, K. *Biochemistry* **2003**, *42*, 14036−14046.

Figure 9. (A) Energy profile of reaction 4: (black line) vacuum, (red line) water, (blue line) wt protein, and (green line) Tyr33 → Phe33 mutant. (B) Same for reaction 5. (C) Same for reaction 6.

previous calculations.[46] The peroxynitrite-coordinated product exhibits the unpaired electron almost totally on the Fe atom and a significant amount of charge donation (0.57 *e*) from peroxynitrite to the metal. In both reactants and products, the quartet state is significantly higher in energy than the doublet state.

The isomerization process leading to nitrate has been proposed to proceed in two steps according to the reactions indicated in eqs 5 and 6. The reaction coordinates chosen to examine the two processes were $\xi_2 = d(O_1 - O_2)$ and $\xi_3 = d(O_1 - N_{NO})$, respectively (Figure 8).

$$Fe(III)[-OONO] \rightarrow Fe(IV)=O + NO_2 \qquad (5)$$

$$Fe(IV)=O + NO_2 \rightarrow Fe(III)[-NO_3^-] \qquad (6)$$

Table 2. Relevant Geometrical (distances in angstroms) and Energetical (ΔE, energy difference between products and reactants, in kcal/mol) Parameters for the NO Addition to the Coordinated O_2 To Yield Nitrite (eq 4) and for the Isomerization Process (eqs 5 and 6)[a]

	Vacuum		Water		Protein	
	reactive	product	reactive	product	reactive	product
	Fe(II)−O_2 + NO → Fe(III)[⁻OONO]					
Fe−O_1	1.83	1.78	1.82	1.80	1.83 (1.84)	1.87 (1.87)
O_1−O_2	1.28	1.45	1.28	1.48	1.32 (1.30)	1.41 (1.40)
O_2−N_{NO}	5.00	1.53	4.45	1.51	3.40 (3.35)	1.60 (1.60)
N_{NO}−O_{NO}	1.18	1.20	1.18	1.19	1.17 (1.18)	1.18 (1.19)
ΔE	−14.6		−20.0		− 23.0 (−21.5)	
	Fe(III)[⁻OONO] → Fe(IV)=O + NO_2					
Fe−O_1	1.78	1.65	1.80	1.67	1.87 (1.87)	1.67 (1.67)
O_1−O_2	1.45	3.40	1.48	2.65	1.41 (1.40)	2.79 (2.72)
O_2−N_{NO}	1.53	1.24	1.51	1.23	1.60 (1.60)	1.24 (1.24)
N_{NO}−O_{NO}	1.20	1.24	1.19	1.23	1.18 (1.19)	1.24 (1.24)
ΔE	−15.7		−18.0		−8.1 (−7.7)	
	Fe(IV)=O + NO_2 → Fe(III)[⁻NO_3]					
Fe−O_1	1.65	1.84	1.67	1.93	1.67 (1.67)	1.94 (1.92)
O_1−N_{NO}	2.52	1.40	3.25	1.46	3.02 (2.99)	1.40 (1.40)
O_2−N_{NO}	1.24	1.25	1.23	1.25	1.24 (1.24)	1.25 (1.25)
N_{NO}−O_{NO}	1.24	1.25	1.23	1.23	1.24 (1.24)	1.25 (1.25)
ΔE	−12.2		−11.7		−18.0 (−19.3)	

[a] For the reactions in protein, values in parentheses correspond to the Tyr33 → Phe33 mutant.

Table 3. Spin Energy Gaps (kcal/mol) and Spin and Mulliken Populations (*e*) of Selected Groups for Relevant Species of Reactions 4−6 in Protein

	Reactive		Approximate Transition Structure		Product	
	spin population	*q*	spin population	*q*	spin population	*q*
	Fe(II)−O_2 + NO → Fe(III)[⁻OONO]					
NO	0.92	0.07				
O_2	−0.75	−0.39				
OONO					0.10	−0.43
Fe	0.88	0.76			0.95	0.80
imidazole	0.00	0.20			0.00	0.26
porphyrin	−0.05	−0.64			−0.05	−0.63
ΔE_{HS-LS}	13.2				23.5	
	Fe(III)[⁻OONO] → Fe(IV)=O + NO_2					
OONO	0.10	−0.43	0.13	−0.47		
NO_2			−0.03	−0.15	−0.82	−0.11
O1			0.16	−0.32	0.70	−0.38
Fe	0.95	0.80	0.93	0.81	1.21	0.80
imidazole	0.00	0.26	0.00	0.23	0.00	0.18
porphyrin	−0.05	−0.63	−0.06	−0.57	−0.09	−0.49
ΔE_{HS-LS}	23.5		29.8		3.3	
	Fe(IV)=O + NO_2 → Fe(III)[⁻NO_3]					
NO_2	−0.82	−0.11	−0.76	−0.11		
O1	0.70	−0.38	0.66	−0.37		
NO_3					0.10	−0.54
Fe	1.21	0.80	1.18	0.80	0.94	0.81
imidazole	0.00	0.18	0.00	0.19	0.00	0.25
porphyrin	−0.09	−0.49	−0.08	−0.50	−0.04	−0.52
ΔE_{HS-LS}	3.3		4.5		16.5	

Although the reaction indicated in eq 5 involves the breaking of the O_1−O_2 bond, it is still exergonic (ΔE values of −15.7, −18.0, −8.1, and −7.7 kcal/mol for vacuum, water, wt protein, and mutant, respectively) and almost barrierless (energy barrier = 1.2 kcal/mol; see Figure 9B). This can be understood by considering that breaking of this bond yields a very stable Fe-(IV)O species, as can be observed by the short Fe−O1 bond distance, which amounts to 1.65 and 1.67 Å in vacuum and in the protein, respectively (Table 2). It can also be noted that the O2−N_{NO} bond becomes significantly shorter in the product compared to the reactant, 1.24 and 1.53 Å, respectively,

consistently with an important stabilization of the product. The analysis of spin and Mulliken populations (Table 3) shows that the peroxynitrite complex breaks homolytically. The doublet species is the ground state. However, the spin energy gap with the quartet state is small. Similar results for spin populations of the oxyferryl compound have been reported for thiolate porphyrin complexes.[62,63]

The reaction described by eq 6 can be analyzed as the addition of a negatively charged O atom coordinated to the heme to the NO_2 radical. The driving force of this reaction is probably related to the formation of a strong O−N bond, as can be seen from Table 2. Inspection of the energy profiles (see Figure 9C) reveals that in all cases, the reaction is exergonic (computed ΔE values of −12.2, −11.7, −18.0, and −19.3 kcal/mol for vacuum, water, wt protein, and mutant, respectively) and proceeds with very small barriers (less than 2.6 kcal/mol). As expected, the product consists of a nitrate ion coordinated to the Fe. The unpaired electron is almost completely located on the metal (Table 3). Experimental results obtained for heme model systems in water solution show that the yield of this reaction is very dependent on the reaction conditions. However, this is due to the fact that the NO_2 radical may escape and react with other species in solution.[60] On the other hand, in the protein, the situation is completely different since NO_2 is trapped in the pocket formed by Phe32, Tyr33, Val36, Phe46, and Val94.

On the basis of the preceding results, it can be concluded that the NO oxidation is a favorable process for the different environments investigated here. Experimental results show that bimolecular rate constants for NO-induced oxidation are similar to those of NO binding to the deoxygenated proteins, showing that the rate-limiting process is ligand diffusion and not the chemical reaction itself.[7] The experimental reaction rate (1 × 10^5 M^{-1} s^{-1}) of peroxynitrite to NO_2 conversion catalyzed by a model porphyrin (FeTMPS) in aqueous solution corresponds to peroxynitrite coordination and subsequent O−O breaking to form the oxyferryl species and NO_2.[60] The peroxynitrite-

(62) Guallar, V.; Friesner, R. A. *J. Am. Chem. Soc.* **2004**, *126*, 8501−8508.
(63) Schöneboom, J. C.; Lin, H.; Reuter, N.; Thiel, W.; Cohen, S.; Ogliaro, F.; Shaik, S. *J. Am. Chem. Soc.* **2002**, *124*, 8142−8151.

coordinated intermediate has not been detected, suggesting that peroxynitrite coordination is rate limiting. Therefore, the bond-breaking process should be much faster, indicating a shallow barrier. Our computed results for reaction 5, which corresponds to O−O bond breaking of the peroxynitrite-coordinated complex, show no energetic barrier and are consistent with the experimental results. The experimental reaction rate for the reaction of an oxyferryl complex with NO_2 has not been measured.[60] However, it has been claimed that it should be faster than NO_2 dimerization, which is a very fast process ($k = 5 \times 10^7 \text{ M}^{-1} \text{ s}^{-1}$). Consistently with this, our results show a small barrier for this process. Finally, the results obtained for the Tyr33 → Phe33 mutant are qualitatively similar to those obtained for the wt protein, thus suggesting that the protein environment, and particularly Tyr33, does not play a significant role in assisting the reaction.

Implications into the Functional Role of trHbN. Similarly to the dioxygenase activity of (flavo)hemoglobins and myoglobin,[64−66] the trHbN enzyme has been suggested to play an essential role in the O_2-sustained NO detoxification.[11] Clearly, understanding of the molecular factors that modulate the efficiency of trHbN is crucial to design therapeutic strategies against diseases, such as human tuberculosis.

One of the factors that have been hypothesized to make a decisive contribution in trHbN is Tyr33, which was argued not only to modulate the O_2 affinity to the heme group but also to develop a catalytic role in the enzyme reaction. This latter role, however, is not supported by the preceding results, as the reaction profile determined for the wt protein is very similar to that obtained for the Tyr33 → Phe33 mutant. Our results point out that Tyr33 is mainly involved in enhancing the oxygen affinity of the protein, which is an important ingredient for determining the NO detoxification ability of the protein, as noted in the enhanced interaction energy of the wt enzyme compared to that in the Tyr33 → Phe33 form. However, besides the energetic contribution due to hydrogen bonding to Tyr33, other factors modulate the O_2 affinity of trHbN. In particular, our results suggest that the donation capacity of His81, enhanced through hydrogen bonding to Met77, might make a relevant contribution.

The analysis of the MD trajectory, as well as the results derived from QM-MM calculations, points out that Tyr33 forms a hydrogen bond with the nitrogen atom of Gln58. The results also indicate that this latter residue does not interact with the O_2 molecule, in agreement with X-ray crystallographic data[15] and resonance Raman spectra.[17] In fact, it must be noted that the occurrence of the Tyr33−Gln58 pair does not necessarily lead to strong stabilization of the heme-bound O_2 in different Hbs.[15,67−69] Nevertheless, present results give support to the suggestion[14,15] that such a hydrogen-bonded interaction is crucial to fix and orient properly the NO molecule with regard to the

heme-bound O_2. In this sense, the hydrogen-bonded network formed by the Tyr33−Gln58 pair might be relevant for the enzyme reaction because of its role in mediating ligand binding stabilization and in assisting the mutual orientation of the reactants in the heme active site.

A more subtle effect might also be envisaged for Tyr33 from the analysis of the MD simulation. Formation of the hydrogen bond between Tyr33 and Gln58, an interaction that was found to be maintained along the whole trajectory, permits anchoring of the B-helix to the E-helix (Tyr33 and Gln58 occupy the B10 and E11 positions in those helices). The results derived from the analysis of the MD trajectory point out the occurrence of conformational transitions leading to the opening of the channel, and that those transitions stem from the interplay between collective "breathing" motions of the protein backbone and local changes in dihedral angles of Phe62, which would eventually facilitate the transition from the closed conformation to the open one. It might, therefore, be speculated that the Tyr33−Gln58 pair-assisted O_2 binding to the heme group modulates the natural dynamics of the protein and regulates in this way the passage of NO through the ligand diffusion tunnel. This hypothesis would be in agreement with experimental data derived from comparison of the resonance Raman spectra in the wt trHbN and the Tyr33 → Phe33 mutant, which indicate that (i) the Tyr33 → Phe33 mutation does not alter the conformational flexibility of the free enzyme, and that (ii) binding to the distal site of the heme group triggers a large-scale conformational change in the enzyme.[19] This hypothetical model would, then, provide a mechanistic model valuable for linking the intrinsic dynamical features of the protein with the ligand binding properties and, ultimately, with the physiological role played by the trHbN enzyme.

Conclusions

The efficiency of the NO oxidation to nitrate by oxygenated trHbN depends on the entry of the reactants NO and O_2 to the distal cavity and on the heme capacity to catalyze the reaction. The results allowed us to identify the opening of the ligand diffusion tunnel, a process controlled by Phe62, which can be considered to be the gate of the channel leading to the heme group in the active site. Moreover, the opening of the tunnel stems from a complex network of conformational changes, which involve both local changes in side chains of specific residues, particularly Phe62, and collective motions of the protein backbone. The results derived from QM-MM calculations indicate that the protein catalyzes the chemical reactions leading to the formation of nitrate mainly by means of the heme group, with no significant contributions of the protein environment. However, our results suggest that the residues that form the binding site, especially the Tyr33−Gln58 pair, might be relevant to the physiological function played by trHbN at three different levels. First, they contribute to modulate the affinity of O_2 and NO ligands. Second, by isolating the reaction intermediates formed transiently in the active site, they prevent other nondesired reactions observed in model porphyrins in aqueous solution from proceeding. Third, the stabilization of the Tyr33−Gln58 pair promoted upon O_2 binding might alter the essential dynamics of the proteins, leading, in turn, to a mechanism for ligand-induced regulation, and eventually to the modulation of the NO detoxification process operative in *M. tuberculosis*.

(64) Poole, R. K.; Hughes, M. N. *Mol. Microbiol.* **2000**, *36*, 775−783.
(65) Flögel, U.; Merx, M. W.; Gödecke, A.; Decking, U. K.; Schrader, J. *Proc. Natl. Acad. Sci. U.S.A.* **2001**, *98*, 735−740.
(66) Frauenfelder, H.; McMahan, B. H.; Austin, R. H.; Chu, K.; Groves, J. T. *Proc. Natl. Acad. Sci. U.S.A.* **2001**, *98*, 2370−2374.
(67) Couture, M.; Das, T. K.; Lee, H. C.; Peisach, J.; Rousseau, D. L.; Wittenberg, B. A.; Wittenberg, J. B.; Guertin, M. *J. Biol. Chem.* **1999**, *274*, 6898−6910.
(68) Das, T. K.; Weber, R. E.; Dewilde, S.; Wittenberg, J. B.; Wittenberg, B. A.; Yamauchi, K.; van Hauwaert, M. L.; Moens, L.; Rousseau, D. L. *Biochemistry* **2000**, *39*, 14330.
(69) Das, T. K.; Couture, M.; Ouellet, Y.; Guertin, M.; Rousseau, D. L. *Proc. Natl. Acad. Sci. U.S.A.* **2001**, *98*, 479−484.

Supporting Information Available: Computational methods and additional optimized geometry figures. This material is available free of charge via the Internet at http://pubs.acs.org.

JA0450004